AN IMPROVED VERSION OF THE ELLIPTIC BLENDING MODEL APPLICATION TO NON-ROTATING AND ROTATING CHANNEL FLOWS

Rémi Manceau
Laboratoire d'études aérodynamiques
UMR 6609, CNRS/Université de Poitiers/ENSMA
SP2MI, Téléport 2, Bd Marie et Pierre Curie, BP 30179
86 962 Futuroscope Chasseneuil cedex, France
remi.manceau@lea.univ-poitiers.fr

ABSTRACT

An improved version of the Elliptic Blending Model, a second moment closure derived from the Elliptic Relaxation Model of Durbin, is applied to non-rotating and rotating channel flows. The model gives very satisfactory results up to very high rotation rates, at least for the highest Reynolds number considered ($Re = 7000$). These results are very encouraging for turbomachinery applications.

INTRODUCTION

In the frame of second moment closure of the Reynolds-averaged Navier–Stokes (RANS) equations, the Elliptic Blending method was introduced by Manceau and Hanjalić (2002) in order to account for the non-local blocking effect of solid boundaries. The method is based on the pioneering ideas of Durbin (1993), which consist in deriving differential equations (called *Elliptic Relaxation equations*) for the redistribution term from a simple modelling of the two-point correlations between velocities and pressure gradients. In order to reduce the number of equations and to get rid of the numerical difficulties linked to the boundary conditions of the Elliptic Relaxation equations, Manceau and Hanjalić (2002) proposed to replace the 6 Elliptic Relaxation equations by a single, Elliptic Blending equation for a "wall-sensitive" quantity α, with the simple boundary conditions $\alpha = 0$ at the walls.

However, the first applications of the Elliptic Blending strategy pointed out some deficiencies of the model (Thielen *et al.*, 2004): numerical instabilities due to the nonlinearity of the Elliptic Blending formula for the dissipation tensor, and a behaviour of the blending function $k\alpha$ far from the wall (where it should strictly go to 1) that was not satisfactory. Moreover, the nonlinear terms behave incorrectly in a rotating reference frame, leading to spurious velocity profiles at moderate rotation rates and numerical divergence at higher rates.

Therefore, an improved version of the Elliptic Blending Model has been developed and results in non-rotating and rotating channels are presented below.

THE MODEL

In the original version of the model, the blending function α was obtained by the following elliptic equation:

$$\alpha - L^2\nabla^2\alpha = \frac{1}{k} \tag{1}$$

and the blending formula for the pressure term ϕ^*_{ij} (velocity-pressure gradient correlation) was:

$$\phi^*_{ij} = (1 - k\alpha)\phi^w_{ij} + k\alpha\phi^h_{ij} \tag{2}$$

where ϕ^h_{ij} is the SSG model (Speziale *et al.*, 1991) and ϕ^w_{ij} a near-wall model. Far from the wall, the differential term in Eq. (1) becomes small compared to the other terms, such that α approaches the value $1/k$: the blending function $k\alpha$ thus approaches 1. However, in many cases, k varies too rapidly to enable this ideal scenario, even far from the wall: the blending function does not strictly go to one.

In the improved version of the model, the elliptic equation reads:

$$\alpha - L^2\nabla^2\alpha = 1 \tag{3}$$

and the blending formula:

$$\phi^*_{ij} = (1 - \alpha^2)\phi^w_{ij} + \alpha^2\phi^h_{ij} \tag{4}$$

Using Eq. (3) ensures that α strictly goes to 1 far from the wall: actually, if the length scale L was a constant, an analytical solution would exist in a flat plate boundary layer: $\alpha(y) = 1 - \exp(-y/L)$.

As mentioned in Manceau and Hanjalić (2002), one of the crucial points of the model is the fact that the blending function $k\alpha$ goes to zero faster than y in the vicinity of a wall: this is the reason why, in the new version, the blending formula involves α^2 (α behaves as y close to a wall).

One of the major objectives of developing the new version is to improve the stability by getting rid of nonlinearities. Firstly, the blending function in the dissipation tensor, $Ak\alpha$ (where A is Lumley's flatness parameter), is also replaced by α^2: the flatness parameter was originally introduced to delay the transition from the near-wall to the far-from-the-wall form, based on *a priori* tests. However, the gain is completely cancelled by the induced numerical instability.

Secondly, as already suggested by Manceau and Hanjalić (2002), the term $C_{\varepsilon 3}\nu\frac{k}{\varepsilon}\overline{u_j u_k}\left(\frac{\partial^2 U_i}{\partial x_j \partial x_k}\right)\left(\frac{\partial^2 U_i}{\partial x_k \partial x_l}\right)$ in the ε equation is replaced by the term given by Eq. (18) (with the new blending function).

Finally, the nonlinear part of the slow term in the SSG model, $g_2\varepsilon\left(b_{ik}b_{kj}-\frac{1}{3}b_{kl}b_{kl}\delta_{ij}\right)$, is removed.

The complete formulation is given below.

EQUATIONS OF THE IMPROVED VERSION OF THE ELLIPTIC BLENDING MODEL

$$\frac{\mathrm{D}\varepsilon}{\mathrm{D}t} = \frac{C'_{\varepsilon_1}P - C_{\varepsilon_2}\varepsilon}{T} + \frac{\partial}{\partial x_l}\left(\frac{C_\mu}{\sigma_\varepsilon}\overline{u_l u_m}T\frac{\partial\varepsilon}{\partial x_m}\right) + \nu\frac{\partial^2\varepsilon}{\partial x_k\partial x_k} \tag{5}$$

$$\frac{\mathrm{D}\overline{u_iu_j}}{\mathrm{D}t} = P_{ij} + G_{ij} + D^\nu_{ij} + D^T_{ij} + \phi^*_{ij} - \varepsilon_{ij} \tag{6}$$

where P_{ij}, D^ν_{ij}, D^T_{ij} and ϕ^*_{ij} stands for the production, the molecular diffusion, the turbulent diffusion and the pressure term (velocity-pressure gradient correlation), respectively. $G_{ij}=-2\boldsymbol{\omega}_k\left(\overline{u_ju_m}\epsilon_{ikm}+\overline{u_iu_m}\epsilon_{jkm}\right)$ is the production arising from the Coriolis acceleration ($\boldsymbol{\omega}_k$ being the rotation pseudo-vector).

$$\phi^*_{ij} = (1-\alpha^2)\phi^w_{ij} + \alpha^2\phi^h_{ij} \tag{7}$$

$$\phi^h_{ij} = -\left(g_1+g_1^*\frac{P}{\varepsilon}\right)\varepsilon b_{ij} + \left(g_3-g_3^*\sqrt{b_{kl}b_{kl}}\right)kS_{ij} + g_4k\left(b_{ik}S_{jk}+b_{jk}S_{ik}-\frac{2}{3}b_{lm}S_{lm}\delta_{ij}\right) + g_5k\left(b_{ik}\Omega_{jk}+b_{jk}\Omega_{ik}\right) \qquad \text{(SSG model)} \tag{8}$$

$$\phi^w_{ij} = -5\frac{\varepsilon}{k}\left[\overline{u_iu_k}n_jn_k+\overline{u_ju_k}n_in_k - \frac{1}{2}\overline{u_ku_l}n_kn_l\left(n_in_j+\delta_{ij}\right)\right] \tag{9}$$

$$\alpha - L^2\nabla^2\alpha = 1 \tag{10}$$

$$\mathbf{n} = \frac{\boldsymbol{\nabla}\alpha}{\|\boldsymbol{\nabla}\alpha\|} \tag{11}$$

$$D^T_{ij} = \frac{\partial}{\partial x_l}\left(\frac{C_\mu}{\sigma_k}\overline{u_lu_m}T\frac{\partial\overline{u_iu_j}}{\partial x_m}\right) \tag{12}$$

$$\varepsilon_{ij} = (1-\alpha^2)\frac{\overline{u_iu_j}}{k}\varepsilon + \frac{2}{3}\alpha^2\varepsilon\delta_{ij} \tag{13}$$

$$S_{ij} = \frac{1}{2}\left(\frac{\partial U_i}{\partial x_j}+\frac{\partial U_j}{\partial x_i}\right) \tag{14}$$

$$\Omega_{ij} = \frac{1}{2}\left(\frac{\partial U_i}{\partial x_j}-\frac{\partial U_j}{\partial x_i}\right)+\epsilon_{mji}\boldsymbol{\omega}_m \tag{15}$$

$$T = \max\left(\frac{k}{\varepsilon}, C_T\left(\frac{\nu}{\varepsilon}\right)^{1/2}\right) \tag{16}$$

$$L = C_L\max\left(\frac{k^{3/2}}{\varepsilon}, C_\eta\frac{\nu^{3/4}}{\varepsilon^{1/4}}\right) \tag{17}$$

$C_{\varepsilon_1}=1.44; C_{\varepsilon_2}=1.83; A_1=0.03; C_\mu=0.21; \sigma_\varepsilon=1.15;$

$\sigma_k=1.0\ ;\ C_L=0.161\ ;\ C_\eta=80.0\ ;\ C_T=6.0\ ;$

$g_1=3.4; g_1^*=1.8; g_3=0.8; g_3^*=1.3; g_4=1.25; g_5=0.4$

$$C'_{\varepsilon_1} = C_{\varepsilon_1}\left(1.+A_1\left(1-\alpha^2\right)\sqrt{\frac{k}{\overline{u_iu_j}n_in_j}}\right) \tag{18}$$

$$\underline{\text{At the wall}}:\quad U_i=0\ ;\ \overline{u_iu_j}=0\ ;\ \varepsilon=2\nu\frac{k}{y^2}\ ;\ \alpha=0 \tag{19}$$

COMPUTATIONAL DETAILS

Computations are performed with a simple, finite-difference, 1D code, using very fine meshes, down to $y^+<0.1$, although, as mentioned by Manceau and Hanjalić (2002), the model is not very sensitive to a coarsening of the near-wall mesh.

NON-ROTATING CHANNEL FLOWS

The calibration of the new version of the model, in particular of the coefficients driving the transition to the near-wall form (C_L, C_T, C_η, A_1) is performed on channel flows at different Reynolds numbers. Fig. 1 shows that the simplified version actually gives better predictions of the mean velocity profiles than the original model, in particular at the highest Reynolds numbers: the present model being more a *near-wall* model than a *low-Reynolds number* model, and the actual industrial applications being generally at high Reynolds numbers, it is believed that the slight misrepresentation of the velocity profile at $Re_\tau=180$ is of minor importance.

Fig. 3(a) shows that the prediction of the Reynolds stresses is also improved, and Fig. 3(b) illustrates the interest of the model: the anisotropies are almost perfectly reproduced, and in particular, the *exact* value $b_{22}=-1/3$ is reached at the wall (two-component limit of turbulence).

Fig. 2(a) shows that the blending function α is virtually independent of the Reynolds number when plotted as a function of y^+. Therefore, the distance over which the wall influences the turbulence scales with ν/u_τ, as the blocking effect does. When α is plotted as a function of y/h (Fig. 2b), it is seen that the region of influence of the wall reduces when the Reynolds number increases, since the shape of α is driven by the turbulent length scale via its elliptic equation (10).

Fig. 4 illustrates, for the components 11 and 22, how the Elliptic Blending Model works. The SSG model is active far from the wall, where $\alpha=1$, and is damped out in the near-wall region by the factor α^2. On the contrary, the near-wall model, derived from asymptotic considerations (for details see Manceau and Hanjalić, 2000), is dominant in the near-wall region, and vanishes further

from the wall, because of the factor $(1-\alpha^2)$. This blending method thus corrects the wrong behaviour of the SSG model in the near-wall region, yielding fairly good budgets of the Reynolds stresses, as shown in Fig. 5.

ROTATING CHANNEL FLOWS

Another objective of the present work is to test the ability of the new version of the Elliptic Blending Model to reproduce the influence of spanwise rotation ($\boldsymbol{\omega} = \{0; 0; \omega\}$), a case relevant to turbomachinery.

This type of flows has been widely investigated in the frame of RANS equations, but scarcely with Reynolds stress models (for recent studies, see for instance Wizman *et al.*, 1996, Pettersson and Andersson, 1997, or Chaouat, 2001). Launder *et al.* (1987) first showed that this closure level is able to reproduce the influence of the Coriolis acceleration on turbulence, just by giving the proper information ($\omega \neq 0$) to the model.

Actually, since the SSG model is written in frame-indifferent variables (b_{ij} and S_{ij} are frame-indifferent, as well as Ω_{ij}, given by Eq. 15), the only necessary modification is the introduction of the *exact* Coriolis production term G_{ij}, arising from the transformation of the equations to rotating coordinates.

The asymptotic considerations on which the near-wall form of the model is based are still valid in a rotating frame, since, in the vicinity of the wall, G_{ij} is negligible in the budget of all the components of the Reynolds stress tensor (in fact, $G_{ij}/\phi^*_{ij} = \mathcal{O}(y^{-1})$ for all i, j). Therefore, the Elliptic Blending Model *does not require any modification* for rotating flows.

The model is evaluated against the DNS ($Re = 2500$, based on the half-width of the channel h) and LES ($Re = 7000$) data of Lamballais *et al.* (1998), which are available for 4 different rotation numbers $Ro = 2\omega h/U_b = 0, 1/6, 0.5, 1.5$. Note that $Ro = 1.5$ is a very high rotation rate, which has never been investigated using second moment closure to the knowledge of the author.

Figs. 6–10 show the influence of the rotation rate on the mean velocity, Reynolds stress and kinetic energy profiles, for the two different Reynolds numbers. The DNS and LES results are globally fairly well reproduced, in particular at $Re = 7000$. The behaviour of all the components when the rotation rate increases is well predicted: decrease of all the components on the cyclonic side (laminarization); initial promotion of turbulence on the anticyclonic side (weak rotation rates) and selective damping for higher rates ($\overline{u^2}$ is damped while $\overline{v^2}$ is enhanced, such that the standard hierarchy of channel flows is inverted: $\overline{v^2} > \overline{u^2}$). At the highest rotation rate, half the channel is completely laminar (e.g., Fig. 10). The laminarization on the cyclonic side is however too strong at $Re = 2500$ for $Ro = 1/6$, mainly due to a rapid decrease of $\overline{u^2}$, and, for $Ro > 0.5$, the laminarization on the anticyclonic side is, on the contrary, underestimated.

The global behaviour of the flow for increasing rotation rates is very well summarized by Fig. 11. It can be seen that on the cyclonic side, the friction velocity decreases linearly with the rotation rate, a result supported by experimental studies (see, e.g., Johnston *et al.*, 1972). A plateau is suddenly reached for a value of Ro depending on the Reynolds number: the behaviour of the model seems to be consistent with the DNS/LES study, although it gives only one point on this plateau. On the anticyclonic side, a sharp increase of the friction velocity is initially obtained, and then a laminarization. It can be seen in Fig. 11(b) that the sensitivity of the friction velocity to the rotation rate is very satisfactory at $Re = 7000$.

Though no numerical/experimental data are available for $Ro > 1.5$, the behaviour of the model has been investigated up to $Ro = 3$: the model predicts a tendency toward complete laminarization. Fig. 12 shows that the mean velocity profile tends to the laminar profile. However, it can be seen in Fig. 13 that a weak turbulence survives on the anticyclonic side, with an unusual structure ($\overline{w^2} > \overline{v^2} > \overline{u^2}$).

Finally, Fig. 14 shows the profiles of the blending function α for increasing rotation rates. This figure is to be compared with Fig. 2(b): when the rotation rate increases, the friction Reynolds number is reduced on the cyclonic side, and consequently the region over which the influence of the wall is felt extends.

CONCLUSION

The new version of the Elliptic Blending Model, which is much more linear than the original version, is also much more numerically stable. Moreover, the predictions in non-rotating channel flows are improved. In the case of rotating channel flows, the model is able to correctly predict the global behaviour of turbulence on both the cyclonic and anticyclonic sides, even though, at low Reynolds number, the laminarization is too strong on the cyclonic side at low rotation rates, and too weak at high rotation rates. Since turbomachinery applications are at high Reynolds numbers, it is believed that these shortcomings are of minor importance: the results at the higher Reynolds number ($Re = 7000$) are very satisfactory.

REFERENCES

B. Chaouat. Simulations of channel flows with effects of spanwise rotation or wall injection using a Reynolds stress model. *J. Fluid Engng.*, 123:2–10, 2001.

P. A. Durbin. A Reynolds stress model for near-wall turbulence. *J. Fluid Mech.*, 249:465–498, 1993.

J. P. Johnston, R. M. Halleen, D. K. Lezius. Effects of spanwise rotation on structure of two-dimensional, fully developed turbulent channel flow. *J. Fluid Mech.*, 56:533, 1972.

E. Lamballais, O. Métais, and M. Lesieur. Spectral-dynamic model for large-eddy simulations of turbulent rotating channel flow. *Theoret. Comput. Fluid Dynamics*, 12:149–177, 1998.

B. E. Launder, D. P. Tselepidakis, and B. A. Younis. A second-moment closure study of rotating channel flow. *J. Fluid Mech.*, 183:63–75, 1987.

R. Manceau and K. Hanjalić. Elliptic blending model: A new near-wall Reynolds-stress turbulence closure. *Phys. Fluids*, 14(2):744–754, 2002.

R. D. Moser, J. Kim, and N. N. Mansour. Direct numerical simulation of turbulent channel flow up to $Re_\tau = 590$. *Phys. Fluids*, 11(4):943–945, 1999.

B. A. Pettersson and H. I. Andersson. Near-wall Reynolds-stress modelling in noninertial frames of reference. *Fluid Dyn. Res.*, 19:251–276, 1997.

C. G. Speziale, S. Sarkar, and T. B. Gatski. Modeling the pressure-strain correlation of turbulence: an invariant

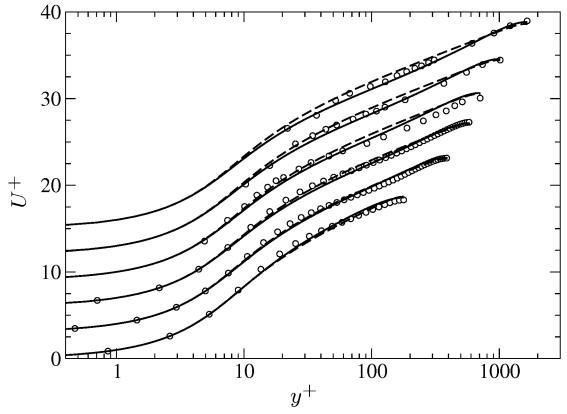

Figure 1: Non-rotating channel flows: mean velocity profiles at different Reynolds numbers. ○ DNS at $Re_\tau = 180, 395, 590$ (Moser *et al.*, 1999) and Exp. at $Re_\tau = 708, 1017, 1655$ (Wei and Willmarth, 1989). ——— New Elliptic Blending Model. ——— Original Elliptic Blending Model. (Profiles are shifted for clarity.)

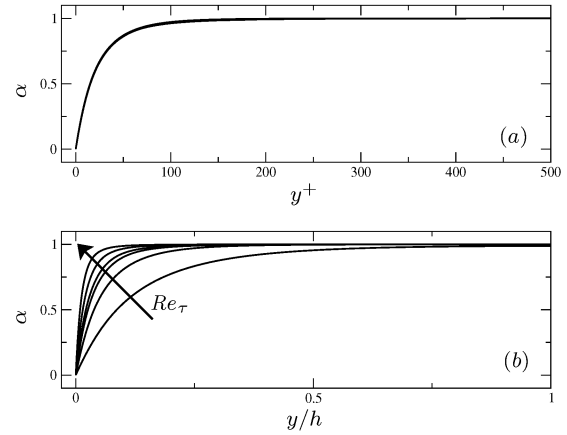

Figure 2: New Elliptic Blending Model in non-rotating channel flows: profiles of the blending function α at different Reynolds numbers ($Re_\tau = 180, 395, 590, 708, 1017, 1655$) plotted as (a): a function of y^+ (profiles are indistinguishable); (b): a function of y/h.

dynamical system approach. *J. Fluid Mech.*, 227:245–272, 1991.

L. Thielen, K. Hanjalić, H. Jonker, and R. Manceau. Predictions of flow and heat transfer in multiple-impinging jets with an Elliptic-Blending second-moment closure. In *Proc. ICHMT Int. Symp. Advances in Computational Heat Transfer, Norway, April 19–24*, CHT–04–263, 2004.

T. Wei and W. W. Willmarth. Reynolds-number effects on the structure of a turbulent channel flow. *J. Fluid Mech.*, 204:57–95, 1989.

V. Wizman, D. Laurence, M. Kanniche, P. Durbin, and A. Demuren. Modeling near-wall effects in second-moment closures by elliptic relaxation. *Int. J. Heat Fluid Flow*, 17(3):255–266, 1996.

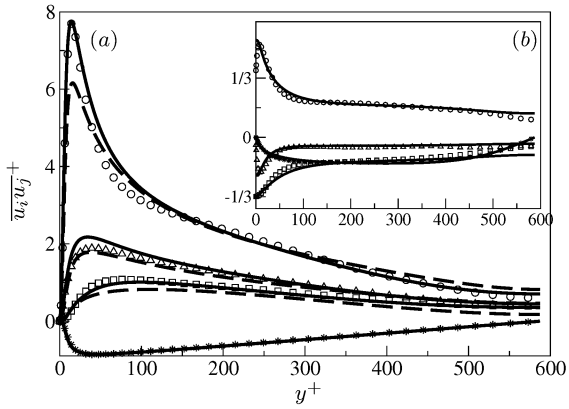

Figure 3: Non-rotating channel flow at $Re_\tau = 590$. Symbols: DNS (Moser *et al.*, 1999). ——— New Elliptic Blending Model ——— Original Elliptic Blending Model. (a) Reynolds stresses (b) Anisotropies (Original model not shown).

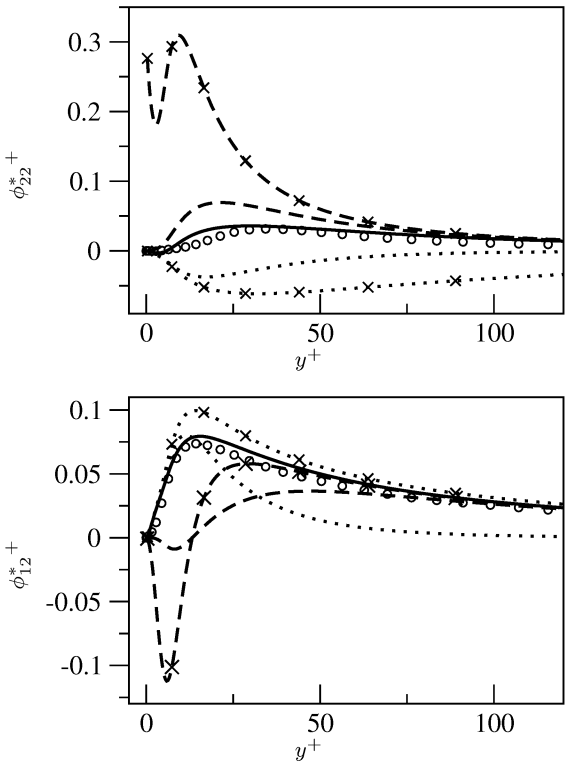

Figure 4: Non-rotating channel flow at $Re_\tau = 590$. Decomposition of the pressure term. ×———× ϕ^h_{ij} (SSG model); ——— $\alpha^2\phi^h_{ij}$; ×-------× ϕ^w_{ij}; ------- $(1-\alpha^2)\phi^w_{ij}$ ——— Total: $\phi^*_{ij} = (1-\alpha^2)\phi^w_{ij} + \alpha^2\phi^h_{ij}$. (a) ϕ^*_{22} (b) ϕ^*_{12}. Symbols: DNS (Moser *et al.*, 1999).

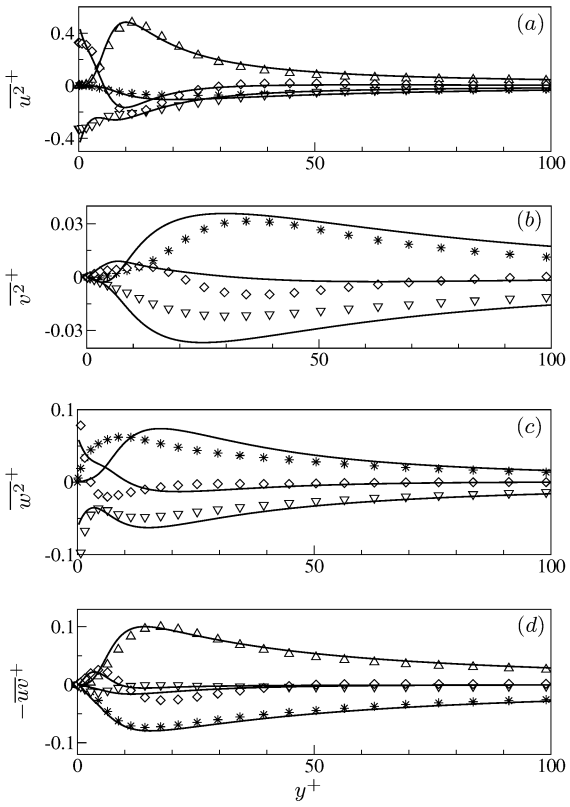

Figure 5: Non-rotating channel flow at $Re_\tau = 590$. Budgets of the Reynolds stresses: (a) $\overline{u^2}$ (b) $\overline{v^2}$ (c) $\overline{w^2}$ (d) $-\overline{uv}$. Symbols: DNS (Moser *et al.*, 1999) ($\triangle$ P_{ij}; $\ast$ ϕ^*_{ij}; $\triangledown$ ε_{ij}; $\diamond$ $D^T_{ij} + D^\nu_{ij}$). —— New Elliptic Blending Model.

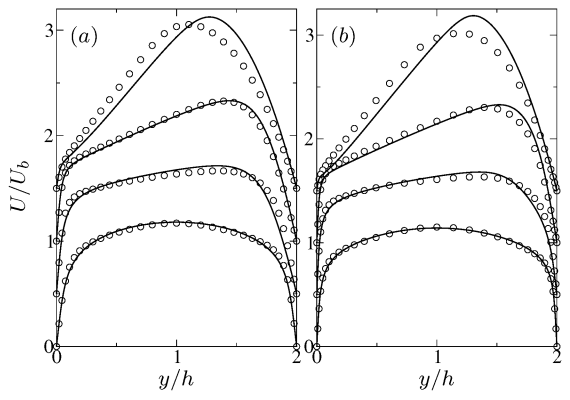

Figure 6: Rotating channel flows. Mean velocity profiles for increasing rotation rates ($Ro = 0, 1/6, 0.5, 1.5$). Profiles are shifted for clarity. (a) $Re = 2500$: ○ DNS (Lamballais *et al.*, 1998) —— New Elliptic Blending Model. (b) $Re = 7000$: ○ LES (Lamballais *et al.*, 1998) —— New Elliptic Blending Model.

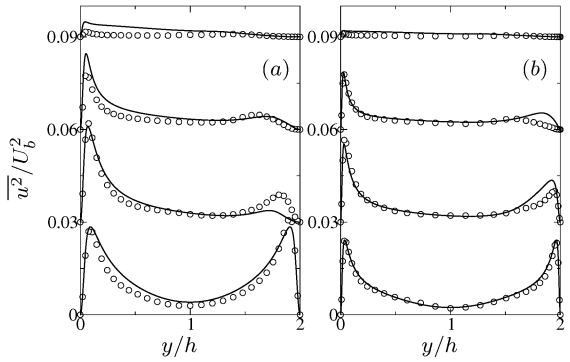

Figure 7: Rotating channel flows. Profiles of $\overline{u^2}$ for increasing rotation rates ($Ro = 0, 1/6, 0.5, 1.5$) (a) $Re = 2500$ (b) $Re = 7000$. Legend: see Fig. 6.

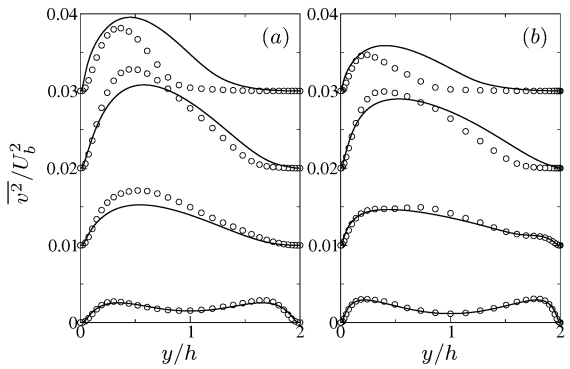

Figure 8: Rotating channel flows. Profiles of $\overline{v^2}$ for increasing rotation rates ($Ro = 0, 1/6, 0.5, 1.5$) (a) $Re = 2500$ (b) $Re = 7000$. Legend: see Fig. 6.

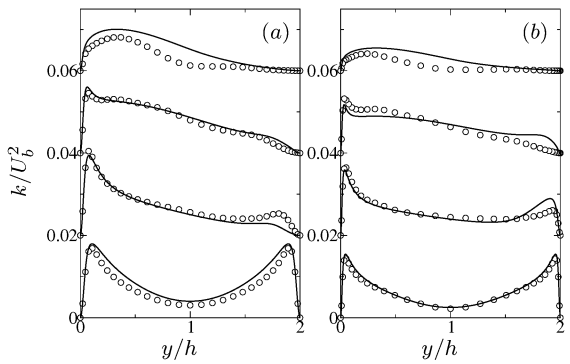

Figure 9: Rotating channel flows. Profiles of turbulent kinetic energy k for increasing rotation rates ($Ro = 0, 1/6, 0.5, 1.5$) (a) $Re = 2500$ (b) $Re = 7000$. Legend: see Fig. 6.

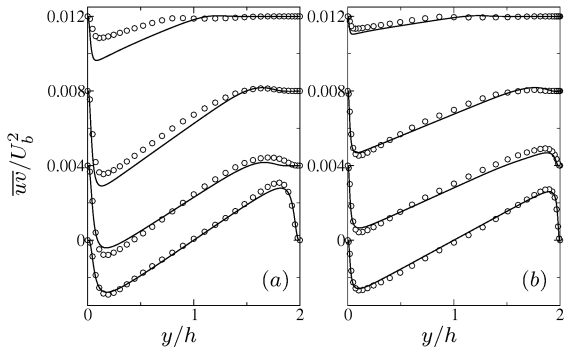

Figure 10: Rotating channel flows. Profiles of turbulent shear stress $\overline{uv}$ for increasing rotation rates ($Ro = 0, 1/6, 0.5, 1.5$) (a) $Re = 2500$ (b) $Re = 7000$. Legend: see Fig. 6.

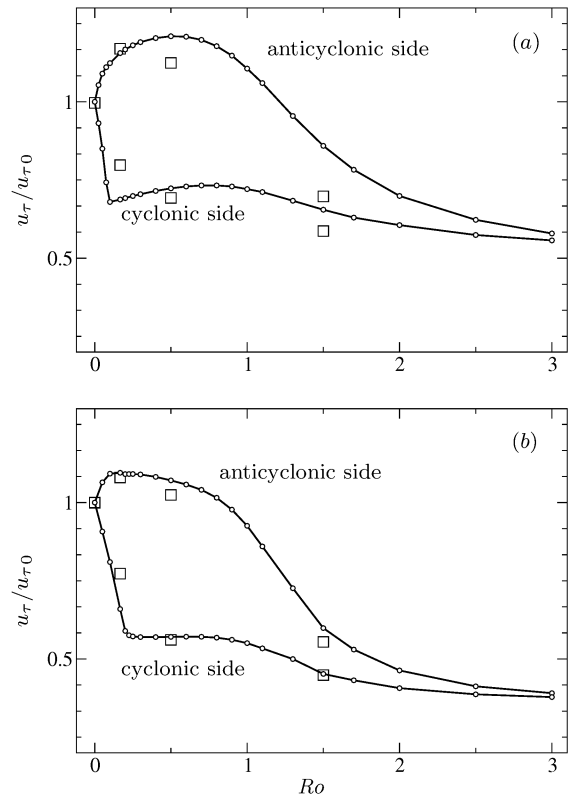

Figure 11: Rotating channel flows at: (a) $Re = 2500$ (b) $Re = 7000$. Effect of rotation rate on wall friction. □ LES (Lamballais *et al.*, 1998); ○——○ New Elliptic Blending Model (each circle represents a computation).

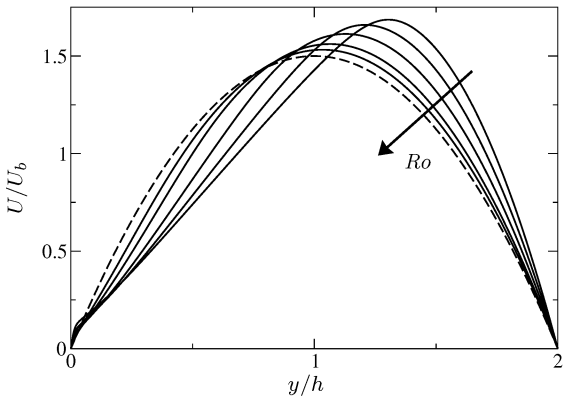

Figure 12: Rotating channel flows at $Re = 7000$. Effect of very strong rotation rates ($Ro = 1.5, 1.7, 2, 2.5, 3$) on the mean velocity profile. —— New Elliptic Blending Model ––– Laminar profile.

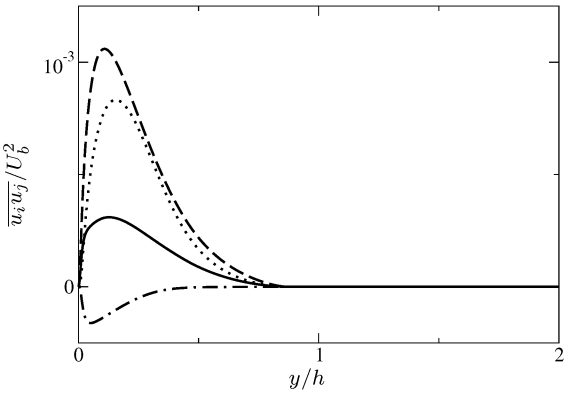

Figure 13: Rotating channel flows at $Re = 7000$. Reynolds stresses at the highest rotation rate investigated ($Ro = 3$). —— $\overline{u^2}$ ------- $\overline{v^2}$ ––– $\overline{w^2}$ -·-·- $\overline{uv}$.

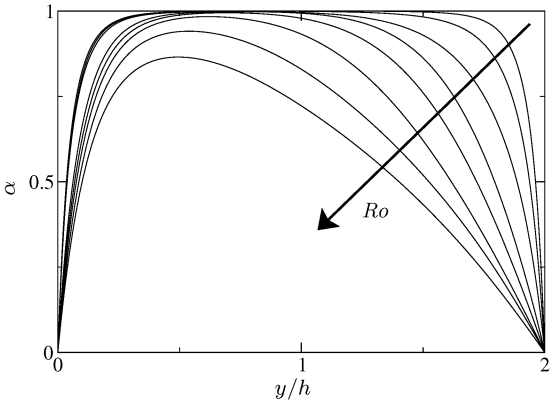

Figure 14: Rotating channel flows at $Re = 7000$. Profiles of the blending function α for increasing rotation rates ($Ro = 0, 1/6, 0.5, 1.5, 1.7, 2, 2.5, 3$).